Monthly Notices of the ROYAL ASTRONOMICAL SOCIETY

MNRAS **447,** 1444–1451 (2015) doi:10.1093/mnras/stu2490

Glycolaldehyde, methyl formate and acetic acid adsorption and thermal desorption from interstellar ices

Daren J. Burke,[1⋆] Fabrizio Puletti,[2] Wendy A. Brown,[1] Paul M. Woods,[3] Serena Viti[4] and Ben Slater[2]

[1]*Division of Chemistry, University of Sussex, Falmer, Brighton BN1 9QJ, UK*
[2]*Department of Chemistry, University College London, 20 Gordon Street, London WC1H 0AJ, UK*
[3]*Astrophysics Research Centre, School of Mathematics and Physics, Queen's University Belfast, University Road, Belfast BT7 1NN, UK*
[4]*Department of Physics and Astronomy, University College London, Gower Street, London WC1E 6BT, UK*

Accepted 2014 November 24. Received 2014 November 21; in original form 2014 November 05

ABSTRACT

We have undertaken a detailed investigation of the adsorption, desorption and thermal processing of the astrobiologically significant isomers glycolaldehyde, acetic acid and methyl formate. Here, we present the results of laboratory infrared and temperature programmed desorption (TPD) studies of the three isomers from model interstellar ices adsorbed on a carbonaceous dust grain analogue surface. Laboratory infrared data show that the isomers can be clearly distinguished on the basis of their infrared spectra, which has implications for observations of interstellar ice spectra. Laboratory TPD data also show that the three isomers can be distinguished on the basis of their thermal desorption behaviour. In particular, TPD data show that the isomers cannot be treated the same way in astrophysical models of desorption. The desorption of glycolaldehyde and acetic acid from water-dominated ices is very similar, with desorption being mainly dictated by water ice. However, methyl formate also desorbs from the surface of the ice, as a pure desorption feature, and therefore desorbs at a lower temperature than the other two isomers. This is more clearly indicated by models of the desorption on astrophysical time-scales corresponding to the heating rate of 25 and 5 $M_{\odot}$ stars. For a 25 $M_{\odot}$ star, our model shows that a proportion of the methyl formate can be found in the gas phase at earlier times compared to glycolaldehyde and acetic acid. This has implications for the observation and detection of these molecules, and potentially explains why methyl formate has been observed in a wider range of astrophysical environments than the other two isomers.

Key words: astrochemistry – molecular processes – methods: laboratory – stars: formation – ISM: molecules – infrared: ISM.

1. INTRODUCTION

The isomers of $C_2O_2H_4$, glycolaldehyde, methyl formate and acetic acid (see Fig. 1) are an important group of complex organic molecules that have been detected in an increasingly wide range of astrophysical environments. These molecules are thought to be important in interstellar chemistry and may also have a role as pre-biotic species (Chyba & Hand 2005).

Glycolaldehyde is the simplest of the monosaccharide sugars. It is a key intermediate in the formose reaction, which involves the formation of sugars, polyols and hydroxy acids from formaldehyde. Ultimately, this autocatalytic reaction can form ribose, which is a central constituent of RNA, and is one of the four macromolecules essential for all forms of life (Cleaves II 2011). Similarly, acetic acid is also of astrobiological interest as it provides a precursor for the formation of the simplest amino acid, glycine. Unlike glycolaldehyde and acetic acid, methyl formate cannot strictly be considered as a pre-biotic molecule. However, it is the most simple ester that has been detected in astrophysical environments and it has been proposed that its presence is closely linked to the formation of dimethyl ether by reaction of methanol (Peeters et al. 2006).

All three isomers have been detected towards Sgr B2, hot molecular cores and hot corinos, all regions containing a large range of saturated organics. The most abundant of the three isomers is methyl formate (Hollis et al. 2001), which was first detected in 1975 (Brown et al. 1975) and has since been detected in numerous astrophysical environments, including high-mass (Macdonald et al. 1996; Favre et al. 2011) and low-mass (Cazaux et al. 2003) hot cores, towards protoplanetary nebula (Remijan et al. 2005) and in comets

⋆E-mail: darenburke@hotmail.com

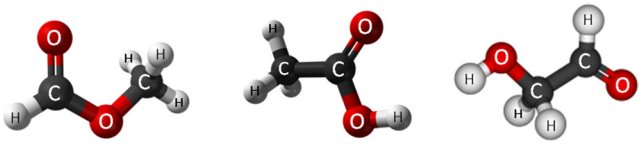

Figure 1. Cartoon showing the different structures of the $C_2O_2H_4$ isomers, methyl formate, acetic acid and glycolaldehyde.

(Crovisier et al. 2004; Remijan et al. 2006). Reported column densities range from 1 to 30 $\times$ 10^{17} cm^{-2} (Liu, Mehringer & Snyder 2001).

Acetic acid was initially detected in 1997 towards Sgr B2(LMH) (Mehringer et al. 1997) and has a lower abundance than methyl formate, with a reported column density of 6.1 $\times$ 10^{15} cm^{-2} in Sgr B2(LMH) (Remijan et al. 2002). Since its initial detection, it has also been observed towards several hot molecular cores including G34.4 + 0.2 (Remijan et al. 2002), G19.61–0.23 and IRAS 16293–2422 with column densities of $\sim$1–2 $\times$ 10^{15} cm^{-2} (Shiao et al. 2010). Until recently, glycolaldehyde was the least abundant of the isomers. It was initially detected in the Galactic Centre towards the hot core Sgr B2(N) (Hollis, Lovas & Jewell 2000) and has since been detected towards hot cores outside the Galactic Centre (Beltrán et al. 2009; Calcutt et. al. 2014), and more recently towards a low-mass binary protostellar system IRAS 16293–2422 (Jørgensen et al. 2012). Estimated column densities of 5.9 $\times$ 10^{13} cm^{-2} (Halfen et al. 2006) and more recently 3–4 $\times$ 10^{16} cm^{-2} (Jørgensen et al. 2012) have been reported. Although not yet detected within comets, Crovisier et al. provided an estimate on the likely upper limit of glycolaldehyde in comet Hale Bopp (Crovisier et al. 2004).

Current estimates of the abundances of the isomers in their respective environments cannot be successfully reproduced by only gas-phase chemical formation pathways. It is therefore thought that grain surface chemistry is an essential component that contributes to both formation and destruction of these molecules (Herbst 2005; Garrod & Herbst 2006; Occhiogrosso et al. 2011; Woods et al. 2012, 2013). This premise has been extended and supported by laboratory studies that have investigated the formation of all three isomers, via the UV and ion irradiation of methanol containing ices (Bennett et al. 2007; Öberg et al. 2009; Modica, Palumbo & Strazzulla 2012; Maity, Kaiser & Jones 2014) and via the destruction of ethylene glycol as a result of proton irradiation (Hudson, Moore & Cook 2005). The destruction of glycolaldehyde and mixed glycolaldehyde and water ices with 0.8-MeV proton ion irradiation has also been studied by infrared spectroscopy (Hudson et al. 2005).

A limited number of experimental studies focusing on the thermal processing of methyl formate and acetic acid in model interstellar ices have been reported in the literature. Bertin et al. (2011) and Lattelais et al. (2011) studied the adsorption and desorption of methyl formate and acetic acid on water ices, focusing mainly on crystalline water ice surfaces at 80 K. A detailed study of acetic acid adsorbed on amorphous water surfaces at 80 K (Bahr et al. 2006) used a combination of metastable impact electron spectroscopy, ultraviolet photoelectron spectroscopy, temperature programmed desorption (TPD) and infrared measurements to explore the interactions between the two ices.

Here, we present the first of a series of papers exploring the thermal processing (adsorption and desorption) of the $C_2O_2H_4$ isomers, glycolaldehyde, methyl formate and acetic acid on a carbonaceous model grain surface. This paper will use the surface science techniques of reflection absorption infrared spectroscopy (RAIRS) and TPD to investigate the properties of the isomers in water-dominated ices. We will show how the isomers are distinguishable in the infrared when embedded in H_2O-rich ices, which is further explored in more detail in a separate paper (Burke et al. in preparation). TPD of isomer and isomer:H_2O ices at astrophysically relevant ice compositions will illustrate how the desorption of each isomer from model grain surfaces is distinct for the three ice configurations: pure, binary layered and binary mixed ices. These results underline the importance of laboratory measurements in guiding the modelling of thermal processing in chemical networks. Incorporating the kinetic parameters obtained from TPD (Burke et al. submitted), a simple model simulating desorption, ice composition and heating rates provides a first approximation of the desorption of the isomers on astrophysical time-scales.

2. EXPERIMENTAL METHODS

Experiments were performed in two separate stainless steel ultra-high vacuum chambers, both of which attained working pressures better than 2 $\times$ 10^{-10} mbar. RAIRS data were recorded in one chamber, whilst TPD were recorded in a second chamber.

In both chambers, HOPG (highly oriented pyrolytic graphite) was used as a model carbonaceous dust grain analogue surface. Sample cleanliness was verified by annealing the sample to 300 K between experiments and monitoring desorption of species from the surface. Sample cooling was achieved by a closed-cycle helium refrigerator (APD cryogenics), which attained base temperatures of around 23 and 20 K for the TPD and RAIRS experiments, respectively.

Methyl formate (Sigma Aldrich), acetic acid (Sigma Aldrich) and deionized water were purified by repeated freeze–pump–thaw cycles prior to deposition onto the HOPG surface via high-precision leak valves. Solid glycolaldehyde dimer (Sigma Aldrich) was placed in a stainless steel vessel and pumped under vacuum (p < 10^{-3} mbar) for several hours prior to heating to 368 K to dose the monomer via a high-precision leak valve. The purity of glycolaldehyde was determined by mass spectrometry. All doses are given in Langmuir (L_m) where 1 L_m = 10^{-6} mbar s. For the mixed and layered binary ices, typically 50 L_m of H_2O was deposited onto the HOPG surface at $\sim$20 K, to form amorphous solid water (ASW). The composition of the co-deposited ices was determined by mass spectrometry.

RAIRS data were recorded with a Thermo-Nicolet spectrometer coupled to a liquid nitrogen cooled mercury cadmium telluride detector. A typical spectrum is comprised of 256 scans, at a resolution of 4 cm^{-1}. All TPD spectra were recorded with a linear heating rate of 0.5 K s^{-1}, controlled via a Eurotherm 2408 interface. A quadrupole mass spectrometer (Hiden) in the line-of-sight mode and differentially pumped was used to detect the desorbing gas flux from the surface. All experiments were repeated several times to ensure reproducibility, including with different mass spectrometer settings. In all cases, the results obtained were identical.

3. RESULTS AND DISCUSSION

3.1 Infrared spectra

Fig. 2 shows a series of infrared spectra recorded for mixtures of the three isomers co-deposited with water in an intimate mixture at a substrate temperature of 20 K. At adsorption temperatures below 140 K, water adopts an amorphous ice configuration, forming ASW (Bolina, Wolff & Brown 2005). The spectra in Fig. 2 clearly show

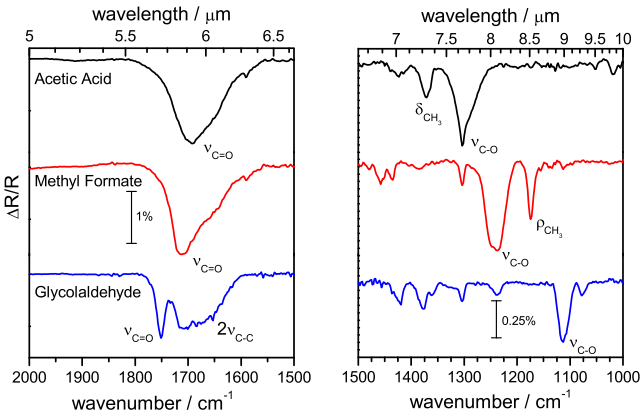

Figure 2. RAIRS of co-deposited 300 L_m $C_2O_2H_4$:H_2O ices deposited on HOPG at 20 K. The left-hand panel focuses on the carbonyl stretch region between 2000 and 1500 cm^{-1}. The right-hand panel shows the fingerprint region between 1500 and 1000 cm^{-1}. The composition of each ice ranges between 20 and 30 per cent.

that the isomers can be distinguished from one another simply on the basis of their infrared spectrum. Note that the O–H stretching region of the spectrum (∼3–3.5 μm) is not shown, as the O–H stretch of the water ice is dominant in this region, and masks the O–H stretching modes of the individual isomers. The left-hand panel shows the spectral region from 5 to 6.6 μm (1500–2000 cm^{-1}) where the most intense band, the C=O stretch, for all three isomers is observed. The appearance of this band is affected by the presence of water in the ice, causing the C=O band to broaden significantly for all of the isomers. Because of this, the bands observed for acetic acid and methyl formate are rather similar; however, glycolaldehyde can be distinguished from the other two isomers due to the additional band observed for the overtone of the C–C band, seen at ∼6 μm. This is in contrast to the infrared spectra for the pure isomers (Burke et al. submitted) which can be clearly distinguished for all three molecules, emphasizing the importance of recording infrared spectra for model ices containing appropriate components.

The right-hand panel shows the fingerprint region of the spectrum for the three isomers (6.5–10 μm, 1000–1500 cm^{-1}). This spectral region is comprised of multiple vibrational modes and will be fully discussed elsewhere (Burke et al. submitted). However, it is clear that in this spectral region the three isomers can be clearly distinguished, even in water-dominated ices. The band that most easily allows the isomers to be identified is the C–O stretching mode, observed at 7.6 μm for acetic acid, 8.1 μm for methyl formate and 9 μm for glycolaldehyde. As seen in the right-hand panel of Fig. 2, there are also a series of smaller vibrational bands, which would allow the isomers to be distinguished from one another. For example for methyl formate, the broad C–O band is observed in conjunction with the CH_3 rocking mode, which occurs to the longer wavelength side of this band. For acetic acid, there is a CH_3 deformation mode, which is always seen to the shorter wavelength side of the sharp C–O band.

3.2 TPD spectra

The thermal desorption behaviour of the three isomers is also distinct, which is illustrated by experimental TPD spectra shown in Figs 3–5 for a range of different ice configurations of the three isomers. For all three isomers, TPD spectra were initially recorded for the pure ice, to characterize the system, in addition to allowing the derivation of kinetic parameters (Burke et al. submitted). Subsequent TPD spectra were then recorded for the isomers in the presence of amorphous water ice, both in a layered configuration (the isomer deposited on top of a thick layer of amorphous water) and in a co-deposited mixture consisting of ∼5 per cent of the isomer in water ice. As can be seen in Figs 3–5, the behaviour of the isomers in the presence of water is very different in each case.

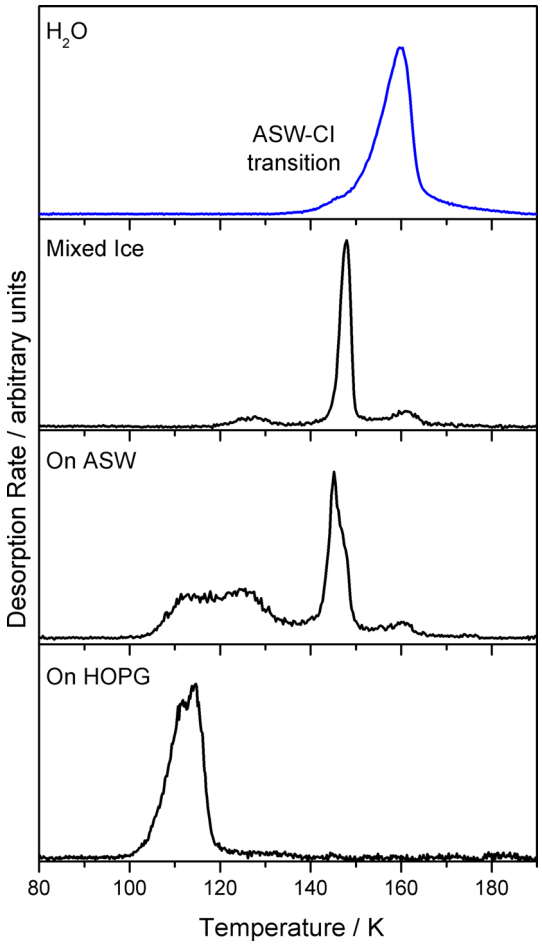

Figure 3. TPD spectra of methyl formate in a range of different ice configurations grown at 23 K. The top spectrum shows the desorption of pure water from the HOPG surface; the second spectrum shows the desorption of methyl formate from an ∼5 per cent co-deposited mixture of methyl formate and water; the third spectrum shows the desorption of 5 L_m methyl formate adsorbed in a layered configuration on top of ASW (the ratio of methyl formate and water is the same as that in the mixed ice) and the bottom spectrum shows the desorption of 5 L_m of pure methyl formate, directly adsorbed on the HOPG surface.

The desorption of methyl formate from all three ice configurations is shown in Fig. 3. A representative H_2O TPD spectrum is shown in the top panel. The low-temperature shoulder on the leading edge of the H_2O TPD spectrum indicates the ASW to crystalline water ice (CI) phase transition of H_2O (Smith et al. 1997). Previous research of volatiles adsorbed on ASW has shown the importance of this phase transition, giving rise to the desorption of trapped gases at higher temperatures when compared to the pure ices. This release at the ASW–CI phase transition has been termed volcano desorption by Smith et al. and has been observed for a wide range of volatiles adsorbed on and within ASW (Ayotte et al. 2001; Collings et al. 2004; Burke & Brown 2010).

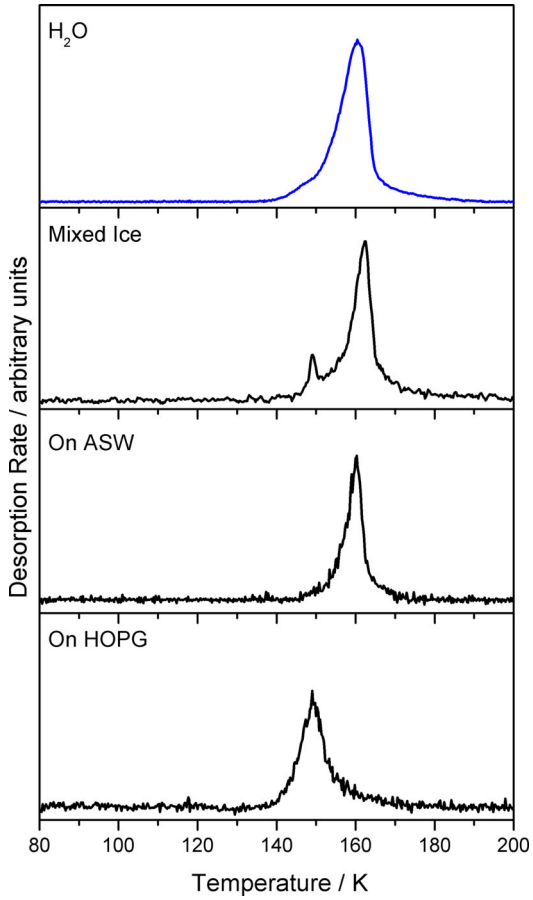

Figure 4. Glycolaldehyde TPD spectra for a range of different ice configurations deposited at 23 K. From top to bottom: TPD spectrum for pure water adsorbed on HOPG; spectrum for the desorption of glycolaldehyde from a 5 per cent co-deposited mixture of glycolaldehyde and water; spectrum showing the desorption of 5 L_m glycolaldehyde adsorbed in a layered configuration on top of ASW; spectrum showing the desorption of 5 L_m of pure glycolaldehyde, directly adsorbed on the HOPG surface.

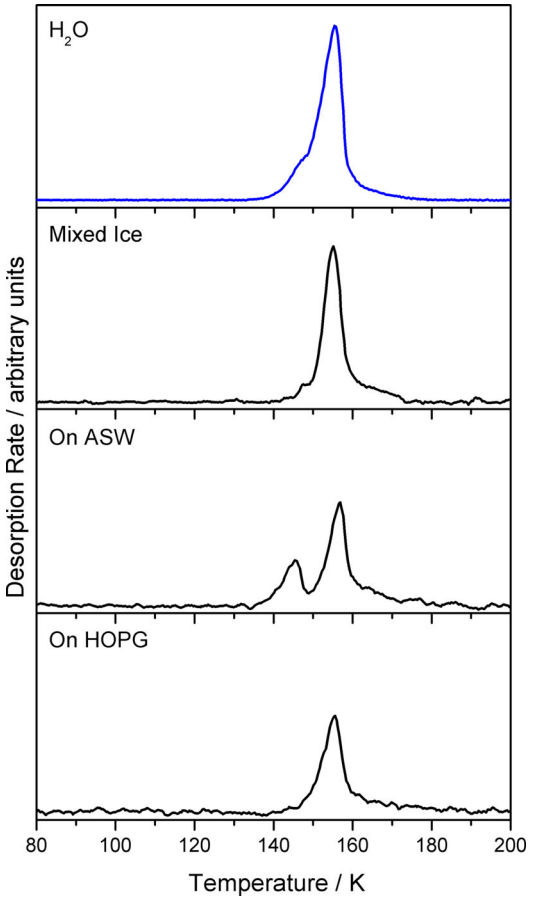

Figure 5. TPD spectra of acetic acid in a range of different ice configurations grown at 23 K. The top spectrum shows the desorption of pure water from the HOPG surface; the second spectrum shows the desorption of acetic acid from a 5 per cent co-deposited mixture of acetic acid and water; the third spectrum shows the desorption of 5 L_m acetic acid adsorbed in a layered configuration on top of ASW; and the bottom spectrum shows the desorption of 5 L_m of pure acetic acid, directly adsorbed on the HOPG surface.

Methyl formate desorption (Fig. 3) is clearly dominated by this volcano desorption mechanism, both for layered and mixed ices. In addition, both systems show the presence of a co-desorption component occurring with the desorption of CI at 160 K. For layered methyl formate ices, a broad peak at lower temperatures (125 K) is also observed, which is assigned to the desorption of methyl formate monolayers bonded directly to ASW (Burke et al. in preparation). This desorption feature is also observed for the mixed ice system, but is less prominent in the TPD spectrum. For the layered methyl formate ice, a further, low-temperature, peak is also observed which can be assigned to the desorption of pure methyl formate multilayers, as observed for the pure methyl formate (bottom spectrum). Evidently, methyl formate desorption is significantly altered by the presence of water ice, compared to desorption when the molecule is directly adsorbed on the graphite surface (bottom panel).

Similarly, glycolaldehyde desorption is also modified by the presence of water, as shown in Fig. 4. However in this case, the desorption of glycolaldehyde is dependent on the ice configuration (layered or mixed). The layered system gives rise to a single glycolaldehyde co-desorption component with CI, whereas the glycolaldehyde mixed ice is characterized by both volcano and co-desorption components. In contrast to methyl formate, glycolaldehyde desorption is dominated by co-desorption with crystalline ice. Again, ASW clearly modifies the desorption of the isomer when compared to the pure ice adsorbed directly on the graphite surface (bottom panel).

Acetic acid desorption behaviour is shown in Fig. 5 and differs from the other two isomers. In the mixed ice configuration, acetic acid gives rise to a solitary co-desorption component with CI and yields the simplest desorption behaviour of the three isomers. The layered system is characterized by two distinct desorption peaks. The higher temperature peak corresponds to acetic acid co-desorption with CI (as also observed in the mixed ices). The lower temperature peak could be a result of volcano desorption; however, the broad peak profile of this feature suggests that is it more likely assigned to a different species. In addition, the desorption temperature of this feature is lower than the corresponding temperature of the ASW–CI transition. This peak is therefore tentatively assigned to the desorption of acetic acid dimers or acetic acid clusters that desorb from the surface of the ASW (Burke et al. in preparation).

The clear differences in the desorption behaviour of the three isomers is summarized in Table 1, which shows the calculated percentages desorbing as surface, volcano and co-desorption peaks from a co-deposited ice at 23 K. As described in the following

section, this data can be used to simulate the desorption of the isomers under astrophysical conditions.

3.3 Simple model of desorption from astrophysical ices

The ultimate objective for all laboratory-based data that explores astronomical processes is to extrapolate the results to simulate astrophysical processes, and hence to provide an experimental basis to describe astronomical modelling. The simple model described below incorporates kinetic desorption parameters and the desorption behaviour of each isomer, both derived from our TPD measurements. These are used to model the desorption of the three isomers from a 0.3-μm-thick mixed ice composed of ASW and the relevant isomer (glycolaldehyde, acetic acid, methyl formate). This thickness has previously been used to measure desorption of ices under astrophysical conditions (Viti et al. 2004; Brown & Bolina 2007).

In our simple model, the rate of the desorption process is described by the Polanyi–Wigner equation:

$$r_{\rm des} = -\frac{{\rm d}\theta}{{\rm d}t} = \upsilon\theta^n \exp\left(-\frac{E_{\rm des}}{RT}\right), \quad (1)$$

where, n, υ and $E_{\rm des}$ are the order of desorption, the pre-exponential factor and desorption energy, θ is the surface coverage, T is the temperature, t is time and R is the gas constant. The kinetic parameters, n, υ and $E_{\rm des}$ are obtained from experimental TPD data using the leading edge analysis that has been described previously (Burke & Brown 2010) and will be discussed more specifically in regard to each isomer in a forthcoming paper (Burke et al. submitted). These values, summarized in Table 2, are derived from data for the pure ices, where desorption is not modified by the presence of H_2O, and are used to simulate desorption of the pure ices.

However, to simulate the desorption of the isomers from H_2O-rich environments, which have a closer analogy to astrophysical ices, clearly the influence of water needs to be considered. As shown in the experimental TPD spectra (Figs 3–5), the desorption of all three isomers is significantly modified by the presence of water, giving rise to additional desorption components in the TPD spectra as a result of the trapping and release of the guest molecules during the ASW–CI phase transition. The proportion of the isomer that desorbs in each separate event (volcano, co-desorption, etc.) is seen in Table 1. As seen in Table 1, the desorption of the isomers in the mixed ices is controlled by water desorption; hence, the kinetic parameters describing pure isomer desorption cannot be used for the mixed ices. Therefore, for the mixed ices, desorption is described by kinetic parameters either for the desorption of ASW (volcano desorption) or CI (co-desorption). The kinetic parameters used in our model are those derived for ASW and CI previously (Fraser et al. 2001). These data are also listed in Table 2.

To model desorption of the mixed ices, the percentage of each desorption component via surface/subsurface desorption, volcano desorption and co-desorption was directly determined from the experimental TPD data. The ratios were determined from the areas under the TPD peaks corresponding to each desorption component as already seen in Table 1. In all cases, the composition of the ice is 99 per cent with respect to H_2O, with the remaining 1 per cent of the ice being composed of the isomer. The desorption constraints, as listed in Table 1, are then placed upon the 1 per cent of molecules corresponding to the isomer in the mixed ice and these are then used to model the total desorption of the different isomers from the ices. Additional ice compositions were also tested (2 and 5 per cent); however, the variations over the range of these three percentages were minimal, and hence we only show data for the 1 per cent mixed ices.

In order to simulate thermal desorption under astrophysical conditions, the ice thicknesses and linear heating rates of 0.5 K s^{-1} used experimentally have to be modified to replicate astrophysical conditions. In our model, the initial total coverage of the ices (both pure isomer ices and mixed isomer:H_2O ices) is set to a value of 9.5×10^{21} mol m^{-2}, corresponding to an ice thickness of 3×10^{-5} m, comparable to estimates of ice thicknesses accreted on dust grains (Brown & Bolina 2007). Whilst mixed ices are the most astrophysically relevant, we have also modelled pure ices of

Table 1. The percentage of each type of desorption that occurs from a binary mixed ice, consisting of mainly water plus the contaminant molecule, grown at 23 K. Data for acetic acid, methyl formate and glycolaldehyde are based on laboratory TPD measurements described here. CO_2 data taken from elsewhere (Edridge et al. 2013).

Molecule	Surface desorption	Volcano desorption with ASW	Co-desorption with CI
Methyl formate	10 per cent	83 per cent	7 per cent
Glycolaldehyde	0 per cent	12 per cent	88 per cent
Acetic acid	0 per cent	0 per cent	100 per cent
CO_2	24 per cent	70 per cent	6 per cent

Table 2. The kinetic parameters used in the model described here. Data for glycolaldehyde, methyl formate and acetic acid were derived from our experimental TPD data and the details are reported elsewhere (Burke et al. submitted). CO_2 data are also derived from our own data and have been published previously (Edridge et al. 2013). Parameters for ASW and CI are those reported by Fraser et al. (2001). Desorption energies are given in K and in kJ mol^{-1}. Note that the units for the pre-exponential factor are those for zero-order desorption.

Molecule	Desorption energy, $E_{\rm des}$ (K)	(kJ mol^{-1})	Desorption order, n	Pre-exponential factor, υ / mol m^{-2} s^{-1}
Methyl formate	4210	35.0	0.01	8.0×10^{33}
Glycolaldehyde	5629	46.8	0.01	2.0×10^{33}
Acetic acid	6615	55.0	0.07	8.0×10^{32}
CO_2	2982	24.8	0.01	1.1×10^{30}
ASW	5605	46.6	0.01	1.0×10^{34}
CI	5761	47.9	0.01	1.0×10^{34}

the same total thickness in order to show the extreme effect that the presence of the water ice has on the desorption of the individual isomers. The pure ices are modelled using multilayer kinetics; therefore, a variation of initial surface coverage/ice thickness will only affect the final desorption temperature of the ice and does not affect the desorption rate. Note that the initial coverage of the water in the ice is of critical importance when modelling desorption on astrophysical time-scales, since the final desorption temperature is dictated by the ice thickness as well as by the heating rate. To provide a comparison of the isomer desorption with the desorption of a more abundant ice component, we have also modelled the desorption of CO_2 from a mixed ice comprised of 10 per cent CO_2 in water ice (the typical composition of CO_2 in the ISM varies from 10 to 37 per cent with respect to water [van Broekhuizen et al. 2006; Whittet et al. 2007]). As for the isomers, Table 1 also shows the percentage of CO_2 desorbing as different components, as determined from experimentally measured TPD data for CO_2:water ices (Edridge et al. 2013).

We will assume that the desorption rate of an ice mantle is determined by the heating rate of a star, which in turn is dictated by the mass of the star which heats the surrounding dust and gas. In our model, the temperature, T, of a star is given by the expression derived previously (Viti et al. 2004):

$$T = At^B, \quad (2)$$

where the values of A and B are determined by the mass of the star and the time, t, is given in years. For our first approximation, heating rates for 5 and 25 $M_\odot$ have been applied to the model. The corresponding values of A and B are $A = 4.856 \times 10^{-2}$ and $B = 0.6255$, $A = 1.766 \times 10^{-4}$ and $B = 1.289$ for 5 and 25 $M_\odot$ respectively. These two masses were chosen to model the effect of different heating rates on the desorption of the isomers. Glycolaldehyde, methyl formate and acetic acid have all been detected towards G31.41 + 0.31 (Beltrán et al. 2005, 2009; Calcutt et al. 2014) which contains a hot core of ∼25 $M_\odot$ (Osorio et al. 2009). Since all three isomers have been observed in a variety of high- and low-mass regions (Cazaux et al. 2003; Shiao et al. 2010; Jørgensen et al. 2012), we have used 5 and 25 $M_\odot$ to represent two types of star.

The results of our simple model of desorption under astrophysical conditions are shown in Figs 6 and 7. Fig. 6 compares the evolution of a pure $C_2O_2H_4$ ice with the desorption of the mixed $C_2O_2H_4$:H_2O ice with a 1 per cent composition for each of the three isomers. In this case, a non-linear heating rate for 25 $M_\odot$ has been applied. For the pure ices (red traces), it is clear that desorption on astrophysical time-scales generates much lower desorption temperatures compared to those observed in the laboratory (Figs 3–5), even when taking account of the different ice thicknesses in the two cases. For example, methyl formate, glycolaldehyde and acetic acid desorb at 77, 108 and 117 K in the model compared to the experimentally measured temperatures of 108, 148 and 155 K, respectively. When the observed experimental constraints of H_2O trapping and release are applied to the model, as expected the model mimics desorption behaviour that is observed in the laboratory. Methyl formate desorbs in three phases, corresponding to the desorption of the pure ice, followed by a dominant phase associated with volcano desorption (ASW) and finally co-desorption with CI. The latter two phases are associated with the desorption of H_2O and occur at higher temperature and on longer time-scales than the desorption of pure methyl formate. Model glycolaldehyde:H_2O mixtures also desorb at higher temperatures/longer time-scales when compared to the pure ices. As seen in Table 1, acetic acid desorption from a

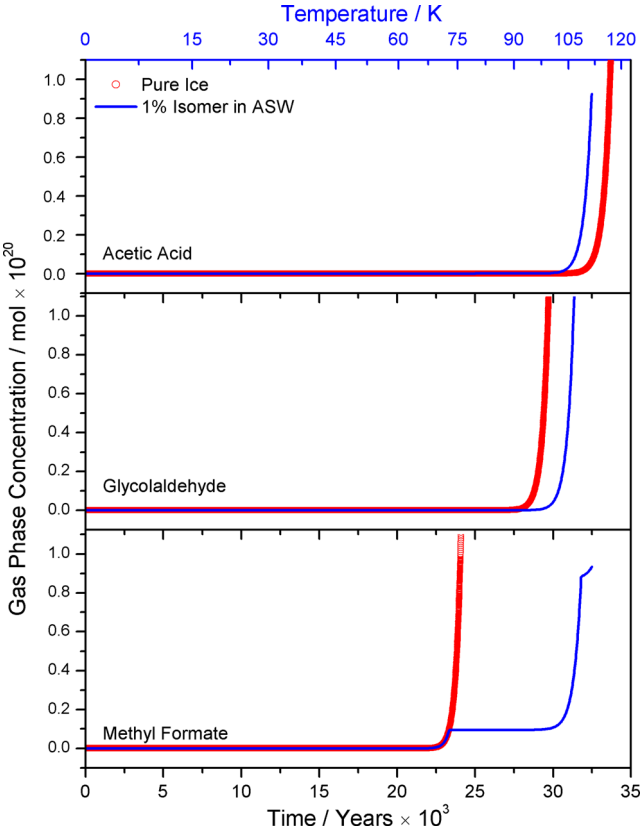

Figure 6. Gas-phase concentration profiles for pure and mixed ice isomers derived from experimental TPD desorption kinetics and using astrophysical time-scales. The top panel shows acetic acid, centre panel glycolaldehyde, bottom panel methyl formate. In each case, pure and 1 per cent mixtures of $C_2O_2H_4$:H_2O are shown. The heating rate is derived from equation (2) for 25 $M_\odot$.

mixed ice is 100 per cent co-desorption and is therefore modelled entirely as CI desorption. The model indicates that co-desorption of acetic acid occurs at a lower temperature/shorter time-scale than that observed for pure acetic acid ices, which is apparently at odds with the experimental TPD results shown in Fig. 5. This effect can be rationalized by the coverage-dependent behaviour of the determined desorption kinetics for acetic acid. A detailed description of this is beyond the scope of this paper and is given elsewhere (Burke et al. in preparation). However, briefly, this observation occurs because the desorption energy of acetic acid (Table 2) is larger than that of water ice, resulting in the desorption of acetic acid at a higher temperature than water, for acetic acid and water ice films of equivalent thickness. However, because acetic acid obeys effectively zero-order desorption kinetics (Table 2), the peak temperature of the desorption increases with increasing ice thickness. Hence, at the lower doses of acetic acid shown in the experimental TPD spectra in Fig. 5, acetic acid desorbs at a lower temperature than water, as expected. In fact experimentally, we observe that very thick acetic acid films do desorb at a higher temperature than water ice films of equivalent thickness, as seen in Fig. 6. Very clearly, the data in Fig. 6 show that there are significant differences between the desorption of the isomers from a mixed ice and from a pure ice, showing the importance of modelling the desorption of these species in the presence of water ice.

Fig. 7 shows the results of the simulation for the 1 per cent $C_2O_2H_4$:H_2O ices as a function of time and stellar mass. For

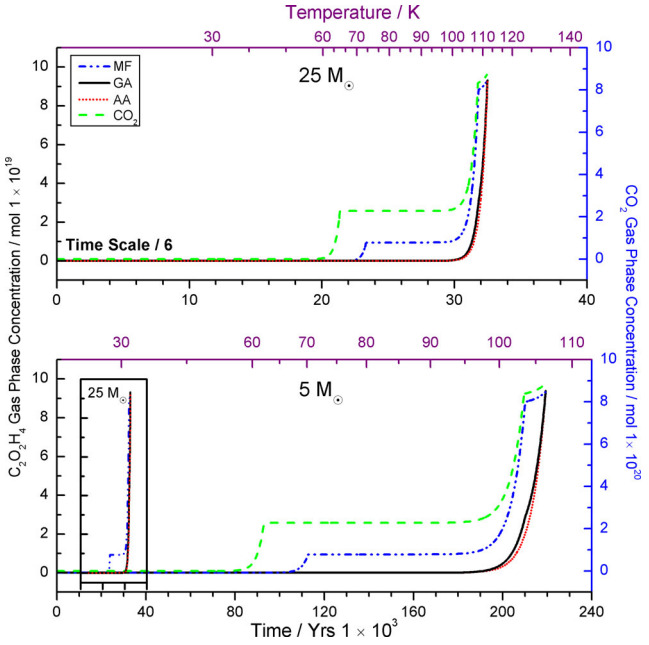

Figure 7. Gas-phase concentration profiles comparing the evolution of 1 per cent $C_2O_2H_4$:H_2O mixed ices for each isomer into the gas-phase employing different astrophysical heating rates. Top panel 25 $M_\odot$, bottom panel shows both 5 $M_\odot$, and an inset for 25 $M_\odot$ to outline the difference in the desorption timescales in the two cases. The evolution has been plotted as a function of time (bottom axis) and temperature (top axis). Note, for the inset only the time axis applies. A 10 per cent CO_2:H_2O evolution trace has been added to the isomer plots to compare the desorption of the isomers to a smaller and more volatile molecule that is typically detected within interstellar ices.

comparison, desorption of a 10 per cent CO_2:H_2O ice, which has been modelled from kinetics derived from experimental TPD data (Edridge et al. 2013), has been included to compare the desorption behaviour of smaller volatiles to that of the $C_2O_2H_4$ isomers. As expected, the faster heating rate of the 25 $M_\odot$ star leads to desorption much earlier than that seen for the 5 $M_\odot$ star. For example, all of the ice desorption has occurred after around 30 000 yr for the 5 $M_\odot$ star, whereas it takes around 220 000 yr for all of the desorption to be complete for the 25 $M_\odot$ star.

The clear difference in the desorption behaviour of the three isomers observed in Fig. 7 is entirely dictated by their different trapping and desorption behaviour in water ice. Methyl formate desorbs earlier than the other two isomers because a distinct component desorbs from the surface/subsurface region of the mixed ice, and therefore, the desorption is not governed by the desorption of water. In contrast, glycolaldehyde and acetic acid only sublimate with the onset of water desorption. However, all three isomers desorb on considerably longer time-scales than the much more volatile CO_2, which shows a reasonably large proportion (24 per cent) of surface desorption, even in a mixed ice. Hence, irrespective of molecular size, methyl formate desorption more closely follows that of CO_2, with a desorption component operating independently of water desorption, and a majority of the trapped species desorbing during the water-phase transition (volcano desorption).

3.4 Astrophysical implications

As clearly outlined by experimental data and by the model presented here, methyl formate thermal desorption behaviour is distinctly different to that of glycolaldehyde and acetic acid. Irrespective of the stellar mass, a proportion of methyl formate desorption occurs at earlier times compared to that of the other two isomers. This is based on methyl formate having a desorption component that is independent of water ice. Hence, based on thermal desorption data alone, this may account for the detection of this isomer in a wider range of objects compared to glycolaldehyde and acetic acid. This may also account for the fact that methyl formate is possibly more extended than the other two isomers in a range of sources (Calcutt et al. 2014). Of particular interest is the detection of methyl formate in colder environments, when compared to star-forming regions (Öberg et al. 2010), since glycolaldehyde and acetic acid have not been detected in these colder regions, to date. Whether the ubiquity of methyl formate arises as a consequence of its thermal desorption behaviour can only be determined for certain once the experimental data from this work are included in chemical models (Woods et al. in preparation).

4. SUMMARY

We have studied the adsorption and thermal desorption of the structural isomers of $C_2O_2H_4$, methyl formate, glycolaldehyde and acetic acid in three different ice configurations: pure isomer ices, binary layered ASW ices and mixed ASW configurations. RAIRS shows that the isomers can be distinguished when embedded in water ice. This is evidenced by changes in the profile and position of key infrared bands, e.g. the C=O stretch at ∼1730 cm^{-1} (∼6 μm) and bands in the fingerprint region of the spectrum (6.6–10 μm). TPD results further confirm the different behaviour of the three isomers during thermal processing and show that they are all strongly influenced by the presence of water ice. Methyl formate exhibits behaviour more similar to a volatile ice component, such as CO_2, with desorption dominated by volcano desorption at low percentages with a small amount of surface desorption being observed. In contrast, glycolaldehyde and acetic acid show similar desorption behaviour that is dictated by the presence of the water ice. The small amount of surface (pure) desorption seen for methyl formate means that it is observed in the gas phase at lower temperatures and on shorter time-scales than the other two isomers, potentially accounting for its observation in a broader range of objects when compared to the other two species.

ACKNOWLEDGEMENTS

The Leverhulme Trust are thanked for funding DJB and PMW to undertake this research at UCL and the University of Sussex are thanked for further funding for DJB at Sussex. FP acknowledges support from the European Community's Seventh Framework Programme FP7/2007-2013 under grant agreement no. 238258. Mark Wilson and Dewi Lewis are thanked for their help with the programming needed for the desorption model.

REFERENCES

Ayotte P., Smith R. S., Stevenson K. P., Dohnálek Z., Kimmel G. A., Kay B. D., 2001, J. Geophys. Res., 106, 387
Bahr S., Borodin A., Höfft O., Kempter V., Allouche A., Borget F., Chiavassa T., 2006, J. Phys. Chem. B, 110, 8649
Beltrán M. T., Cesaroni R., Neri R., Codella C., Furuya R. S., Testi L., Olmi L., 2005, A&A, 435, 901
Beltrán M. T., Codella C., Viti S., Neri R., Cesaroni R., 2009, ApJ, 690, L93

Bennett C. J., Chen S. H., Sun B., Chang A. H. H., Kaiser R. I., 2007, ApJ, 660, 1588
Bertin M., Romanzin C., Michaut X., Jeseck P., Fillion J.-H., 2011, J. Phys. Chem. C, 115, 12920
Bolina A. S., Wolff A. J., Brown W. A., 2005, J. Phys. Chem. B, 109, 16836
Brown R. D., Crofts J. G., Gardner F. F., Godfrey P. D., Robinson B. J., Whiteoak J. B., 1975, ApJ, 197, L29
Brown W. A., Bolina A. S., 2007, MNRAS, 374, 1006
Burke D. J., Brown W. A., 2010, Phys. Chem. Chem. Phys., 12, 5947
Calcutt H., Viti S., Codella C., Beltrán M. T., Fontani F., Woods P. M., 2014, MNRAS, 443, 3157
Cazaux S., Tielens A. G. G. M., Ceccarelli C., Castets A., Wakelam V., Caux E., Parise B., Teyssier D., 2003, ApJ, 593, L51
Chyba C.F., Hand K.P., 2005, ARA&A, 43, 31
Cleaves H. J., II, 2011, in Gargaud M., Amils R., Cernicharo Quintanilla J., Cleaves H. J., II, Irvine W. M., Pinti D. L., Viso M., eds, Encyclopedia of Astrobiology. Springer, Berlin, p. 600
Collings M. P., Anderson M. A., Chen R., Dever J. W., Viti S., Williams D. A., McCoustra M. R. S., 2004, MNRAS, 354, 1133
Crovisier J., Bockelée-Morvan D., Colom P., Biver N., Despois D., Lis D. C., 2004, A&A, 418, 1141
Edridge J. L., Freimann K., Burke D. J., Brown W. A., 2013, Phil. Trans. R. Soc. A, 371, 20110578
Favre C., Despois D., Brouillet N., Baudry A., Combes F., Guélin M., Wootten A., Wlodarczak G., 2011, A&A, 532, A32
Fraser H. J., Collings M. P., McCoustra M. R. S., Williams D. A., 2001, MNRAS, 327, 1165
Garrod R. T., Herbst E., 2006, A&A, 457, 927
Halfen D. T., Apponi A. J., Woolf N., Polt R., Ziurys L. M., 2006, ApJ, 639, 237
Herbst E., 2005, J. Phys. Chem. A, 109, 4017
Hollis J. M., Lovas F. J., Jewell P. R., 2000, ApJ, 540, L107
Hollis J. M., Vogel S. N., Snyder L. E., Jewell P. R., Lovas F. J., 2001, ApJ, 554, L81
Hudson R. L., Moore M. H., Cook A. M., 2005, Adv. Space Res., 36, 184
Jørgensen J. K., Favre C., Bisschop S. E., Bourke T. L., van Dishoeck E. F., Schmalzl M., 2012, ApJ, 757, L4
Lattelais M. et al., , 2011, A&A, 532, A12
Liu S.-Y., Mehringer D. M., Snyder L. E., 2001, ApJ, 552, 654
Macdonald G. H., Gibb A. G., Habing R. J., Millar T. J., 1996, A&AS, 119, 333
Maity S., Kaiser R. I., Jones B. M., 2014, Faraday Discuss., 168, 485
Mehringer D. M., Snyder L. E., Miao Y., Lovas F. J., 1997, ApJ, 480, L71
Modica P., Palumbo M. E., Strazzulla G., 2012, Planet. Space Sci., 73, 425
Öberg K. I., Garrod R. T., van Dishoeck E. F., Linnartz H., 2009, A&A, 504, 891
Öberg K. I., Bottinelli S., Jørgensen J. K., van Dishoeck E. F., 2010, ApJ, 716, 825
Occhiogrosso A., Viti S., Modica P., Palumbo M. E., 2011, MNRAS, 418, 1923
Osorio M., Anglada G., Lizano S., D'Alessio P., 2009, ApJ, 694, 29
Peeters Z., Rodgers S. D., Charnley S. B., Schriver-Mazzuoli L., Schriver A., Keane J. V., Ehrenfreund P., 2006, A&A, 445, 197
Remijan A., Snyder L. E., Liu S.-Y., Mehringer D., Kuan Y.-J., 2002, ApJ, 576, 264
Remijan A. J., Wyrowski F., Friedel D. N., Meier D. S., Snyder L. E., 2005, ApJ, 626, 233
Remijan A.J. et al., , 2006, ApJ, 643, 567
Shiao Y.-S.J., Looney L. W., Remijan A. J., Snyder L. E., Friedel D. N., 2010, ApJ, 716, 286
Smith R. S., Huang C., Wong E. K. L., Kay B. D., 1997, Phys. Rev. Lett., 79, 909
Van Broekhuizen F. A., Groot I. M. N., Fraser H. J., van Dishoeck E. F., Schlemmer S., 2006, A&A, 451, 723
Viti S., Collings M. P., Dever J. W., McCoustra M. R. S., Williams D. A., 2004, MNRAS, 354, 1141
Whittet D. C. B., Shenoy S. S., Bergin E. A., Chiar J. E., Gerakines P. A., Gibb E. L., Melnick G. J., Neufeld D. A., 2007, ApJ, 655, 332
Woods P. M., Kelly G., Viti S., Slater B., Brown W. A., Puletti F., Burke D. J., Raza Z., 2012, ApJ, 750, 19
Woods P. M., Slater B., Raza Z., Viti S., Brown W. A., Burke D. J., 2013, ApJ, 777, 90

This paper has been typeset from a TEX/LATEX file prepared by the author.